Muon spin rotation measurements of the vortex state in vanadium: A comparative analysis using iterative and analytical solutions of the Ginzburg-Landau equations

M. Laulajainen,[1] F. D. Callaghan,[1] C. V. Kaiser,[1] and J. E. Sonier[1,2,*]
[1]*Department of Physics, Simon Fraser University, Burnaby, British Columbia, Canada V5A 1S6*
[2]*Canadian Institute for Advanced Research, 180 Dundas Street West, Toronto, Ontario, Canada M5G 1Z8*
(Received 24 April 2006; revised manuscript received 26 June 2006; published 29 August 2006)

We report muon spin rotation measurements on a single crystal of the marginal type-II superconductor V. The measured internal magnetic field distributions are modeled assuming (i) solutions of the Ginzburg-Landau (GL) equations for an ideal vortex lattice obtained using an iterative procedure developed by Brandt [Phys. Rev. Lett. **78**, 2208 (1997)], (ii) a variational GL method, and (iii) a modified London model. Remarkably the models yield qualitatively similar results. The magnetic penetration depth λ and the coherence length ξ determined from the data analysis exhibit strong field dependences, which are attributed to changes in the electronic structure of the vortex lattice. We find that the zero-field extrapolated value of λ is essentially independent of the assumed model and agrees well with the value obtained by experimental techniques that probe the Meissner state. On the other hand, only fits to either of the GL models yield reliable values of ξ.

DOI: 10.1103/PhysRevB.74.054511 PACS number(s): 74.20.De, 74.25.Ha, 74.25.Qt, 76.75.+i

I. INTRODUCTION

In order to analyze muon spin rotation (μSR) measurements on a type-II superconductor in the vortex state, it is necessary to assume a theoretical model for the spatial variation of the local internal magnetic field $B(\mathbf{r})$.[1] An essential requirement of the model is that it must account for the finite size of the vortex cores. Thus far the internal magnetic field distribution $n(B)$ measured by μSR has been analyzed assuming analytical models for $B(\mathbf{r})$ based on London and Ginzburg-Landau (GL) theories. Since London theory does not account for the finite size of the vortex cores, a cutoff factor derived from GL theory must be inserted into the analytical London expression for $B(\mathbf{r})$ to correct for the divergence of $B(\mathbf{r})$ as $r \rightarrow 0$. Unfortunately, analytical cutoff factors are derivable from GL theory only near the lower and upper critical fields B_{c1} and B_{c2}. At intermediate fields, these analytical cutoffs deviate substantially from the precise numerical calculations,[2] making modified London models inappropriate for the analysis of μSR data. There are several approximate analytical expressions for $B(\mathbf{r})$ that have been derived from the GL equations.[3–6] For example, a variational solution of the GL equations[3,4] has proven to be a reliable model for analyzing μSR measurements on V_3Si (Ref. 7), $NbSe_2$ (Ref. 8), and $YBa_2Cu_3O_{7-\delta}$ (Refs. 9 and 10). However, this analytical GL model is strictly valid only at low reduced fields $b=B/B_{c2}$ and large values of the GL parameter κ. Thus, often used analytical models for $B(\mathbf{r})$ have limited validity and can deviate substantially from the numerical solutions of the GL equations.

Brandt has developed an iterative method for solving the GL equations that accurately determines $B(\mathbf{r})$ for arbitrary b, κ, and vortex-lattice symmetry.[11] Thus far this iteration method has not been applied to the analysis of μSR measurements of $n(B)$ in the vortex state. As a first test of this method we have chosen to study the marginal type-II superconductor vanadium (V). This rigorous analysis method is expected to be required for V, whose low value of κ falls outside the range of validity of the analytical models. In addition, the low value of B_{c2} ($\approx$0.45 T) gives us experimental access to reduced fields which are beyond the range of validity of the analytical model.

The paper is organized as follows: Theoretical models for $B(\mathbf{r})$ are described in Sec. II. The experimental procedures are described in Sec. III. Measurements in zero external magnetic field are presented in Sec. IV. Measurements in the vortex state are described in Sec. V, and concluding remarks are given in Sec. VI.

II. THEORETICAL MODELS

A. Iterative GL solution

Here we briefly outline the iteration method presented in Ref. 11, and correct some typographical errors contained therein. The GL equations are written in terms of the real order parameter ω, the local magnetic field B, and the supervelocity $\mathbf{Q}$, which are expressed as the Fourier series

$$\omega(\mathbf{r}) = \sum_{\mathbf{K}} a_{\mathbf{K}}(1 - \cos \mathbf{K}\cdot\mathbf{r}), \tag{1}$$

$$B(\mathbf{r}) = \bar{B} + \sum_{\mathbf{K}} b_{\mathbf{K}} \cos \mathbf{K}\cdot\mathbf{r}, \tag{2}$$

$$\mathbf{Q}(\mathbf{r}) = \mathbf{Q}_A(\mathbf{r}) + \sum_{\mathbf{K}} b_{\mathbf{K}} \frac{\hat{\mathbf{z}}\times\mathbf{K}}{K^2} \sin \mathbf{K}\cdot\mathbf{r}, \tag{3}$$

where $a_{\mathbf{K}}$ and $b_{\mathbf{K}}$ are Fourier coefficients, $\omega(\mathbf{r})=|\psi(\mathbf{r})|^2$, $\bar{B}$ is the average internal field, and $\psi(\mathbf{r})$ is the complex GL order parameter. The "tail" of the position vector $\mathbf{r}=(x,y)$ is at the vortex center $(0,0)$. The local magnetic field B is given in units of $\sqrt{2}B_c$ (where B_c is the thermodynamic critical field), and all length scales are in units of the magnetic penetration depth λ. $\mathbf{Q}_A(\mathbf{r})$ is the supervelocity obtained from Abrikosov's solution of the GL equations near B_{c2}:

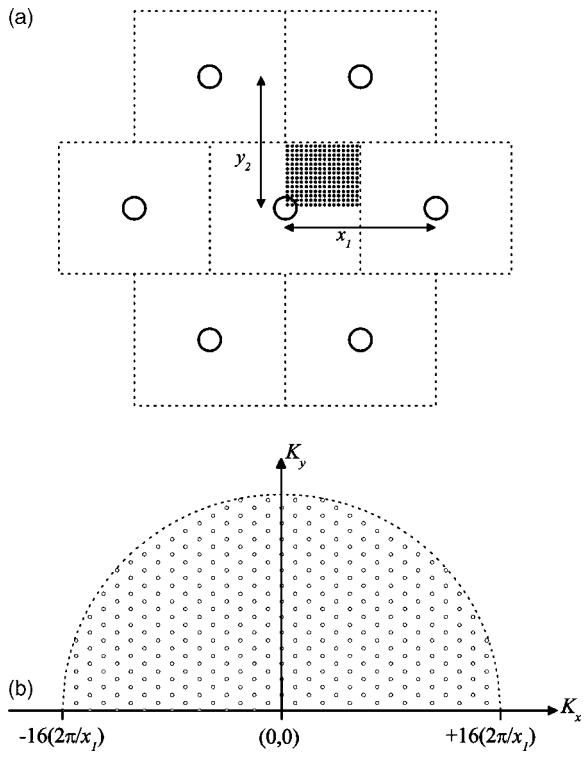

FIG. 1. (a) The vortex positions in the hexagonal lattice (○) and the rectangular unit cell (dotted lines). Due to symmetry, the theoretical probability field distribution $n(B)$ was calculated at approximately 950 locations (•) within just one-quarter of the rectangular unit cell. For the sake of clarity, the sampled positions are shown at 1/4 of the density used in the calculations. (b) The points in the reciprocal space lattice (◦) that are included in the **K** sums of Eqs. (1)–(3), Eqs. (11) and (12).

$$\mathbf{Q}_A(\mathbf{r}) = \frac{\nabla \omega_A \times \hat{\mathbf{z}}}{2\kappa\omega_A}, \tag{4}$$

where $\omega_A(\mathbf{r})$ is calculated from Eq. (1) using

$$a_{\mathbf{K}}^A = -(-1)^{\nu} \exp(-\pi\nu\sqrt{3}). \tag{5}$$

Here $\nu = m^2 + mn + n^2$, assuming a hexagonal vortex lattice with vortex positions given by

$$\mathbf{R}_{mn} = (mx_1 + nx_2, ny_2), \tag{6}$$

where m and n are integers, x_1 is the intervortex spacing, $x_2 = x_1/2$, and $y_2 = x_1\sqrt{3}/2$. The spatial field profile $B(\mathbf{r})$ was calculated at approximately 950 locations within one-quarter of the rectangular unit cell shown in Fig. 1(a). The reciprocal lattice vectors used in the calculation of $B(\mathbf{r})$ are given by

$$\mathbf{K} \equiv \mathbf{K}_{mn} = \frac{2\pi}{S}(my_2, nx_1 + mx_2), \tag{7}$$

where S is the unit cell area. The $\mathbf{K}_{mn}$ vectors are restricted to those indicated in Fig. 1(b), corresponding to $-16 \geq m \leq 16$ and $-16 \geq n \leq 16$ within a semicircle with $K_y \geq 0$ (but excluding vectors with $K_x \geq 0$ and $K_y = 0$). It was found that the calculated field distribution did not change significantly if the summation was extended to values of $|n|$ and $|m|$ greater than 16.

The Fourier coefficients $a_{\mathbf{K}}$ and $b_{\mathbf{K}}$ are calculated from

$$a_{\mathbf{K}} = \frac{4\kappa^2\langle(\omega^2 - 2\omega + \omega Q^2 + g)\cos \mathbf{K}\cdot\mathbf{r}\rangle}{K^2 + 2\kappa^2}, \tag{8}$$

$$a_{\mathbf{K}} = a_{\mathbf{K}}\langle\omega - \omega Q^2 - g\rangle/\langle\omega^2\rangle, \tag{9}$$

$$b_{\mathbf{K}} = \frac{-2\langle[\omega B + \bar{\omega}(\bar{B} - B) + p]\cos \mathbf{K}\cdot\mathbf{r}\rangle}{K^2 + \bar{\omega}}, \tag{10}$$

where $g = (\nabla\omega)^2/(4\kappa^2\omega)$, $\bar{\omega}$ is the spatial average of ω, and $p = (\nabla\omega \times \mathbf{Q})\hat{\mathbf{z}} = Q_y\frac{\partial\omega}{\partial x} - Q_x\frac{\partial\omega}{\partial y}$. We note that the definitions of p and the $\bar{\omega}(\bar{B} - B)$ term in Eq. (10) are incorrectly written in the original article,[12] but have been corrected here. As explained in Ref. 11, solutions to the GL equations are acquired by first iterating Eqs. (1), (8), and (9) a few times to relax ω and then iterating Eqs. (10), (1)–(3), (8), and (9), and again (10), etc., to relax B.

B. Comparison with other models

Here we compare the results of the above iteration method for $B(\mathbf{r})$ to the widely used modified London and analytical GL models. The local magnetic field at position $\mathbf{r} = (x, y)$ in the modified London model[13] is

$$B(\mathbf{r}) = \bar{B}\sum_{\mathbf{K}} \frac{e^{-i\mathbf{K}\cdot\mathbf{r}} e^{-K^2\xi^2/2(1-b)}}{1 + \lambda^2 K^2/(1-b)}. \tag{11}$$

Although this model is considered applicable for reduced fields $b = B/B_{c2} \leq 0.25$ and $\kappa \geq 2$, the Gaussian cutoff factor $\exp[-K^2\xi^2/2(1-b)]$ introduced to account for the logarithmic divergence of $B(\mathbf{r})$ at the center of the vortex is not strictly valid.[2]

The approximate analytical solution of the GL equations for $B(\mathbf{r})$ is[4]

$$B(\mathbf{r}) = \bar{B}(1 - b^4)\sum_{\mathbf{K}} \frac{e^{-i\mathbf{K}\cdot\mathbf{r}} u K_1(u)}{\lambda^2 K^2}, \tag{12}$$

where

$$u^2 = 2\xi^2 K^2(1 + b^4)[1 - 2b(1-b)^2]. \tag{13}$$

K_1 is a modified Bessel function, and ξ is the GL coherence length. This analytical GL model is a reasonable approximation for $b \ll 1$ and $\kappa \gg 1$.

Figures 2–4 show comparisons between the solutions for $B(\mathbf{r})$ from the three different models, plotted along the straight line connecting nearest-neighbor vortices. The parameters used to generate the curves in Fig. 2 are characteristic of the high-κ superconductor V_3Si (Ref. 7). While there

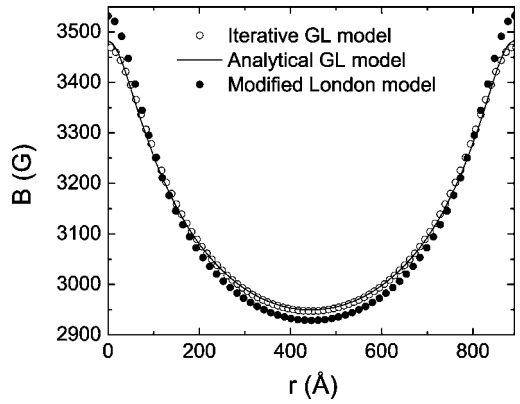

FIG. 2. The spatial field profile $B(r)$ along the straight line connecting nearest-neighbor vortices, for a hexagonal vortex lattice, $\kappa=25$, $\bar{B}=3$ kG, and $\lambda=1000$ Å.

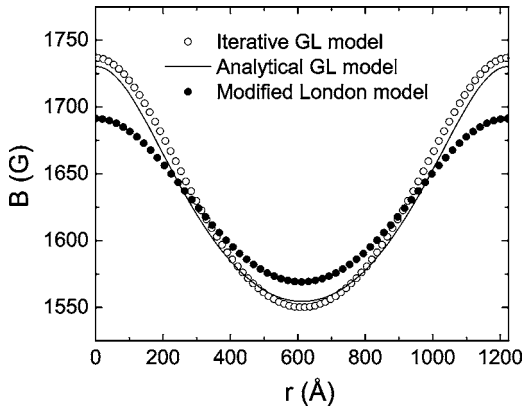

FIG. 4. The spatial field profile $B(r)$ along the straight line connecting nearest-neighbor vortices, for a hexagonal vortex lattice, $\kappa=5.3$, $\bar{B}=1.6$ kG, and $\lambda=1042$ Å.

is good agreement between the iterative and analytical solutions of the GL equations, the modified London model deviates substantially both in the region of the vortex cores and midway between the cores. Figure 3 shows that the modified London and analytical GL models completely break down for $\kappa=1/\sqrt{2}$, the limit of type-II superconductivity. For example, in the case of the analytical GL model, there is actually a region between the vortices where the local field changes direction. In Fig. 4, plots of $B(\mathbf{r})$ are shown for a set of parameters obtained from μSR measurements on the low-κ superconductor V (see Sec. V). The value $\kappa=5.3$ is rather large for V, but as we explain in Sec. V, κ is really an "effective" fit parameter influenced by the electronic structure of the vortex lattice. Generally, it can be seen from Figs. 2–4 that the overall agreement between the models improves as κ increases.

III. EXPERIMENTAL DETAILS

The single crystal of the low-κ superconductor V measured in the present study was purchased from Goodfellow Cambridge Ltd.[14] The crystal is a disk, 13 mm in diameter by 0.35 mm thick, with the $\langle 111\rangle$ crystallographic direction perpendicular to the plane of the disk. Magnetization measurements indicate that the crystal has a superconducting transition temperature of $T_c=5.2$ K and an upper critical field of $H_{c2}\approx 4.2$ kOe. This value of H_{c2} corresponds to a BCS coherence length of $\xi_0\approx 280$ Å. A four-probe potentiometric ac resistivity measurement yielded $\rho=0.7$ $\mu\Omega$ cm just above T_c, which is 31 times smaller than ρ at room temperature. Using the carrier concentration $n\approx 9\times 10^{28}$ m^{-3} obtained from Hall resistance measurements,[15] a free-electron-theory[16] calculation of the mean free path yields $l=\hbar k_F/\rho n e^2\approx 900$ Å, where $k_F=(3\pi^2 n)^{1/3}$ is the Fermi wave number and e is the electronic charge. Thus our sample is in the clean limit with $l/\xi_0\approx 3$. Neutron scattering measurements performed on our V single crystal showed no evidence of an intermediate mixed state (i.e., a mixture of Meissner and vortex-lattice phases).[17]

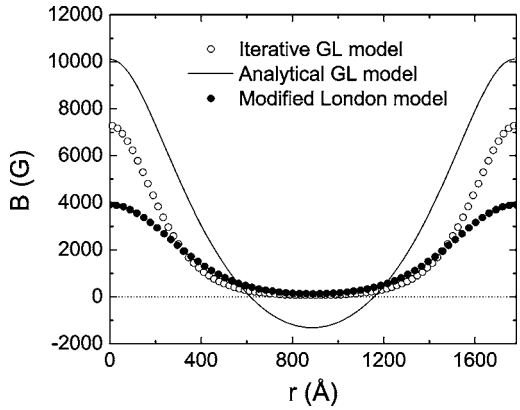

FIG. 3. The spatial field profile $B(r)$ along the straight line connecting nearest-neighbor vortices, for a hexagonal vortex lattice, $\kappa=1/\sqrt{2}$, $\bar{B}=753$ G, and $\lambda=150$ Å.

The μSR measurements were carried out on the M15 beamline at the Tri-University Meson Facility (TRIUMF), Vancouver, Canada, using a dilution refrigerator to cool the sample. Measurements of the vortex state were done under field-cooled conditions in a "transverse field" (TF) geometry, in which the magnetic field was applied along the z axis parallel to the $\langle 111\rangle$ direction of the crystal, but perpendicular to the initial muon spin polarization $P_x(0)$ (which defines the x axis). Each measurement was done by implanting approximately 2×10^7 spin-polarized muons one at a time into the crystal, where their spins precess around the local magnetic field $B(\mathbf{r})$ at the Larmor frequency $\omega=\gamma_\mu B$, where $\gamma_\mu=0.0852$ μs^{-1} G^{-1} is the muon gyromagnetic ratio. The muons stop randomly on the length scale of the vortex lattice and hence evenly sample $B(\mathbf{r})$. The μSR signal obtained by the detection of the decay positrons from an ensemble of muons implanted into the single crystal is given by

$$A(t)=a_0 P_x(t), \tag{14}$$

where $A(t)$ is called the μSR "asymmetry" spectrum, a_0 is the asymmetry maximum, and $P_x(t)$ is the time evolution of the muon spin polarization:

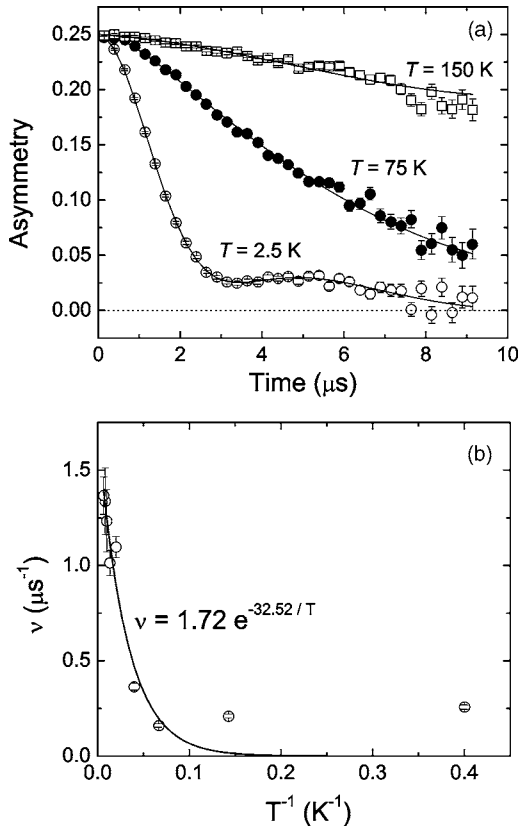

FIG. 5. (a) Representative asymmetry spectra (symbols) acquired in V in zero external magnetic field and fits (solid lines) to the numerical dynamic Gaussian Kubo-Toyabe function. (b) The temperature dependence of the extracted muon hop rate ν (circles). The solid line is a fit to $\nu(T \geq 15\ \mathrm{K})$ using an Arrhenius function.

$$P_x(t) = \int_0^\infty n(B)\cos(\gamma_\mu B t + \phi)dB. \tag{15}$$

Here ϕ is a phase constant and

$$n(B') = \langle \delta(B' - B(\mathbf{r})) \rangle, \tag{16}$$

is the probability of finding a local field B in the z direction at an arbitrary position $\mathbf{r}$ in the x-y plane. Further details of this application of the μSR technique are found in Ref. 1.

IV. ZERO-FIELD MEASUREMENTS

Figure 5(a) shows asymmetry spectra for our V sample in zero external magnetic field. These spectra contain a 7% time-independent background contribution from muons stopping outside the sample. The signal coming from muons stopping inside the sample is well described by a numerical dynamic Gaussian Kubo-Toyabe function.[18] This function is characterized by a relaxation rate Δ corresponding to the width of the internal magnetic field distribution experienced by the muons and a parameter ν corresponding to the hop rate of the muons in the sample. As shown in Fig. 5(b), the muon hop rate in our V crystal decreases with decreasing temperature to $\nu \approx 0.2\ \mu\mathrm{s}^{-1}$ at $T=15$ K $(1/T \approx 0.07\ \mathrm{K}^{-1})$. At $T \geq 15$ K, the data are well described by the classical Arrhenius law for thermally activated motion in the presence of potential barriers:[18]

$$\nu = \nu_0 \exp(-E_a/k_B T), \tag{17}$$

where k_B is Boltzmann's constant, E_a is the activation energy for thermally assisted muon hopping, and ν_0 is a constant. Fitting the $T \geq 15$ K data using this expression yields $\nu_0 = 1.72\ \mu\mathrm{s}^{-1}$ and $E_a = 4.5$ meV. Below $T=15$ K there is perhaps a slow increase in the hop rate ν, which we speculate is due to quantum mechanical tunneling as observed in other metals.[19]

Assuming that the muon occupies an interstitial site of tetrahedral symmetry in the V crystal lattice, we can calculate the muon diffusivity D_μ from the expression[18]

$$D_\mu = \nu \frac{a^2}{24}, \tag{18}$$

where $a=3.02$ Å is the lattice constant. This gives $D_\mu \approx 9.7 \times 10^{-16}\ \mathrm{m}^2/\mathrm{s}$ at $T=2.5$ K. Brandt and Seeger performed a thorough theoretical study of the effect of muon diffusion on μSR line shapes in the vortex state.[20] They found that muon diffusion causes significant smearing of the sharp features of $n(B)$ for values of D_μ greater than $\approx 10^{-3}\gamma_\mu |M| d^2$, where M is the sample magnetization and d is the intervortex spacing. Our measured muon diffusivity is several orders of magnitude smaller than this. At $H=1.6$ kOe, for example, we have $\gamma_\mu |M| d^2 \approx 2 \times 10^{-8}\ \mathrm{m}^2/\mathrm{s}$, which means that $D_\mu (\approx 9.7 \times 10^{-16}\ \mathrm{m}^2/\mathrm{s}) = 5 \times 10^{-8} \gamma_\mu |M| d^2$. Thus muon diffusion has a negligible effect on the μSR linehapes measured here.

V. MEASUREMENTS IN THE VORTEX STATE

A. Comparison of fits

To fit the μSR signals in the vortex state, the field distribution $n(B)$ contained in the theoretical polarization function $P_x(t)$ of Eq. (15) was generated from one of the three theoretical models for $B(\mathbf{r})$ described in Sec. II. Recent neutron scattering measurements on the same V sample[17] have allowed us to assume an ideal hexagonal vortex lattice in our analysis. In addition, $P_x(t)$ was multiplied by a Gaussian function $\exp(-\sigma^2 t^2/2)$, which is equivalent to convoluting $n(B)$ with the Gaussian $(\gamma_\mu/\sigma\sqrt{2\pi})\exp(-\gamma_\mu^2 B^2/2\sigma^2)$. This accounts for disorder in the vortex lattice,[21] and the static local-field inhomogeneity created by the large ^{51}V nuclear dipole moments. An additional Gaussian depolarization function was added to Eq. (14) to account for approximately 20% of the signal arising from muons that stopped outside the sample.

A typical asymmetry spectrum at $H=1.6$ kOe and $T=2.6$ K is displayed in Fig. 6. The solid curve through the data is a fit assuming the solution of $B(\mathbf{r})$ obtained from the iterative GL method. The parameter values obtained from this fit were used to calculate the spatial field profiles shown in Fig. 4. Fourier transforms of typical time domain signals and fits to both the iterative and analytical GL models are shown in Figs. 7 and 8. From the Fourier transforms one can see that both fits capture the main features of the μSR line

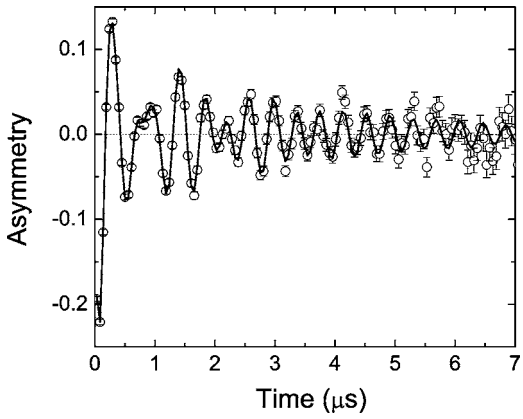

FIG. 6. Time evolution of the muon spin polarization (circles) in V at $H=1.6$ kOe and $T=2.6$ K and a fit (solid curve) assuming the solution of $B(\mathbf{r})$ from the iterative GL method.

shape and are of high quality. In particular, for the data in Fig. 7 the ratio of χ^2 to the number of degrees of freedom (NDF) is comparable, being 1.26 for the fit to the iterative GL solution and 1.30 for the fit to the analytical GL model. The values of λ, ξ, and σ extracted from the two models differed by 9%, 8%, and 13%, respectively. We note that despite returning significantly different parameter values in some cases, fits with both models resulted in similar values of χ^2/NDF for all of the data presented in this article.

Interestingly, the results from the two models are in slightly better agreement at the lowest temperatures and magnetic fields. For example, at $H=1.2$ kOe and $T=0.02$ K, the differences in λ, ξ, and σ are 7%, 8%, and 2%, respectively. On the other hand, at $H=2.9$ kOe and $T=0.02$ K, λ, ξ, and σ differ by 10%, 9%, and 3%, respectively. Even so, the quality of the fits is about the same for both models. This is evident from the Fourier transforms shown in Fig. 8. At high reduced field b, the values of λ and ξ obtained from the iterative GL method are likely to be more accurate, since at these high fields the analytical GL model is being applied outside its range of validity. The fits using the modified London model were of similar quality to those using the GL models.

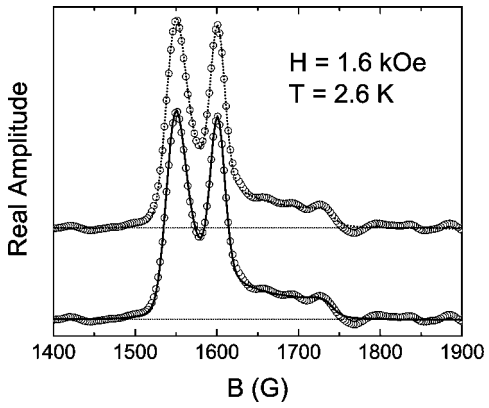

FIG. 7. Fourier transforms of the muon spin precession signal in V at $H=1.6$ kOe and $T=2.6$ K (circles), the fit using the iterative GL solution (solid curve), and the fit to the analytical GL model (dotted curve). The peak at 1600 G is the background signal originating from muons that missed the sample.

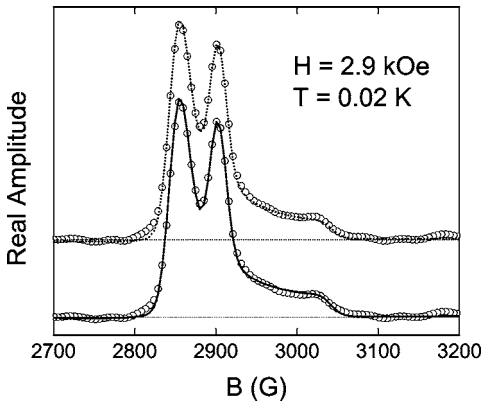

FIG. 8. Fourier transforms of the muon spin precession signal in V at $H=2.9$ kOe and $T=0.02$ K (circles), the fit using the iterative GL solution (solid curve), and the fit to the analytical GL model (dotted curve). The peak near 2900 G is the background signal originating from muons that missed the sample.

In the following two sections, complete results for fits using both the iterative and analytical GL models as well as the modified London model are presented. There we show that despite differences in the absolute values of λ and ξ, fits to the two GL models yield similar temperature and magnetic field dependences for these length scales. In particular, we show that the value of λ extrapolated to zero field is, within experimental uncertainty, the same for both GL models and agrees well with Meissner state measurements on V using other experimental techniques. In addition, the magnetic field dependences of λ and ξ obtained from the London model are very similar to the results from the GL models. However, the results for the temperature dependences of these length scales deviate noticeably from those obtained using the GL models.

B. Temperature dependences of λ and ξ

Fourier transforms of the muon spin precession signal from V at $H=1.6$ kOe and temperatures below T_c are shown in Fig. 9. Magnetization measurements indicate that $T_c=3.65$ K at $H=1.6$ kOe. As the temperature is lowered, the μSR line shape broadens and the amplitude of the high-field "tail" decreases. While the high-field cutoff is less obvious at $T=0.02$ K, we note that the "true" cutoff in $n(B)$ is smeared out by the Fourier transform.[1] In fact the fits in the time domain are quite sensitive to the high-field tail, yielding finite values for ξ, even at $T=0.02$ K.

Figures 10 and 11 show the temperature dependences of $1/\lambda^2$, σ, and ξ determined from our fits of the muon spin precession signals at $H=1.6$ kOe, assuming solutions for $B(\mathbf{r})$ from the iterative and analytical GL methods and the modified London model. Despite the differences in absolute values of $1/\lambda^2$, both GL data sets in Fig. 10 are well described by BCS weak-coupling $1/\lambda^2(T)$ curves[22] for $T_c=3.65$ K. $1/\lambda^2(T)$ from the London model, however, is not well described by a BCS curve and deviates most substan-

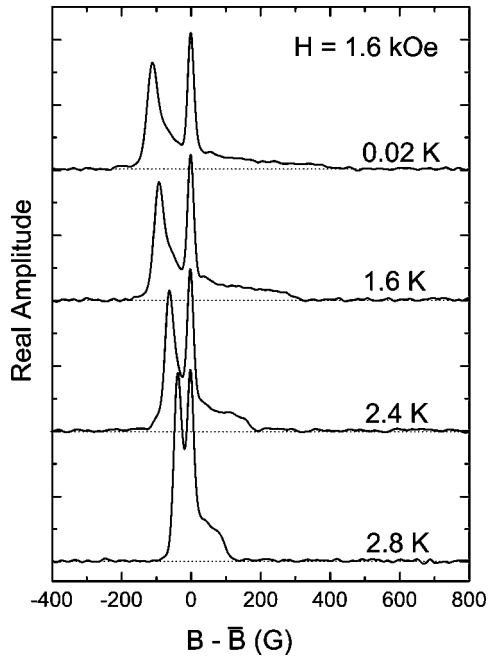

FIG. 9. Fourier transforms of the muon spin precession signal in V at $H=1.6$ kOe and $T<T_c(H)=3.65$ K.

tially from the expected trend at $T>2.4$ K. In addition, we note that a satisfactory fit could not be obtained at $T=3.2$ K with the London model. The inset in Fig. 10 shows that all three models yield similar values for the additional broadening parameter σ. As λ becomes longer with increasing temperature, there is a greater overlap of the vortices and a corresponding reduction in the pinning-induced disorder of the vortex lattice. This is because the energy associated with the interaction between vortex lines depends on λ.[23] For this reason $\sigma(T)$ roughly follows $1/\lambda^2$ in Fig. 10.

The temperature dependence of the coherence length ξ is shown in Fig. 11. ξ is a measure of the vortex core size. Recently, we have demonstrated from μSR and thermal conductivity measurements on BCS superconductors[7,8] that the core size is dependent on the degree of localization of the

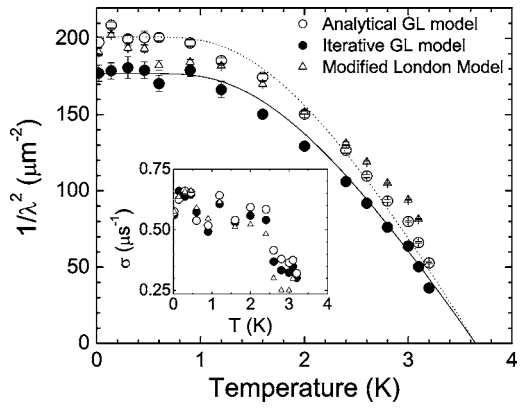

FIG. 10. Temperature dependence of $1/\lambda^2$ in V at $H=1.6$ kOe, determined from fits using the iterative and analytical GL models and the modified London model. The solid and dotted curves are theoretical BCS weak-coupling predictions for $T_c=3.65$ K.

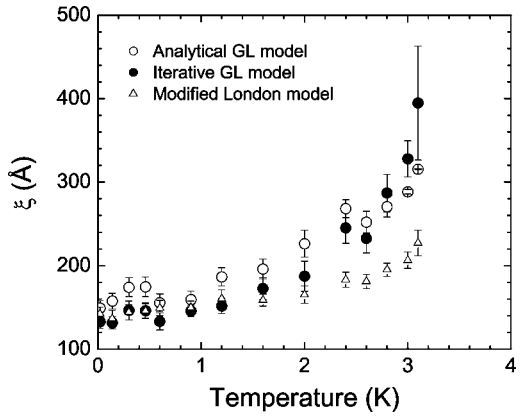

FIG. 11. Temperature dependence of ξ in V at $H=1.6$ kOe, determined from fits using the iterative and anlytical GL models and the modified London model.

quasiparticle bound core states. Thermal depopulation of the more spatially extended high-energy core states results in a shrinking of the core size with decreasing temperature. This is the so-called "Kramer-Pesch effect,"[24] which has previously been observed in $NbSe_2$ by μSR (Refs. 9 and 25) and shown to be dependent on magnetic field.[26] In a clean BCS type-II superconductor the core size of an isolated vortex is expected to be temperature independent below $T\sim T_c/k_F\xi_0$, where k_F is the Fermi wave number and ξ_0 is the BCS coherence length. We see in Fig. 11 that $\xi(T)$ obtained from the fits to all models displays the Kramer-Pesch effect, with ξ saturating below $T\approx 1$ K. Compared with the GL models, however, ξ obtained from the London model displays a weaker temperature dependence above $T\approx 1.2$ K. Using the free-electron expression $k_F=(3\pi^2 n)^{1/3}$ (Ref. 16) and $n\approx 9\times 10^{28}$ m^{-3} from Hall resistance measurements,[15] we obtain $k_F\approx 1.4\times 10^{10}$ m^{-1}. Assuming the value of the superconducting coherence length $\xi_0\approx 280$ Å estimated from the extrapolated zero-temperature value of H_{c2}, the core size in our V crystal is therefore theoretically expected to saturate below $T\approx 10^{-2}$ K. The premature saturation of the core size observed in Fig. 11 could result from quasiparticle scattering by nonmagnetic impurities,[27] but this is unlikely given that our sample is in the clean limit. It is important to note that theoretical predictions only exist for isolated vortices.[24,27,28] In a lattice, the core states of nearest-neighbor vortices overlap to some degree, and this is likely the reason why the strength of the Kramer-Pesch effect observed by μSR weakens with increasing field.[26] The delocalization of core states due to vortex-vortex interactions and the corresponding reduction in the core size also explain why the low-temperature value of ξ in Fig. 11 is much smaller than ξ_0.

C. Magnetic field dependences of λ and ξ

In Fig. 12, Fourier transforms of the muon spin precession signal in V at $T=0.02$ K are shown for different applied magnetic fields $H<H_{c2}$. The changes in the μSR line shape as a function of H are similar to those previously observed in $NbSe_2$ (Ref. 29) and result directly from the change in vortex density. Increasing the vortex density reduces the internal

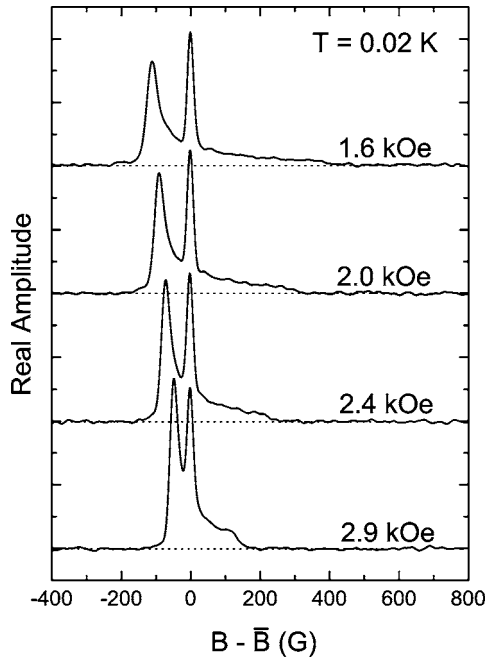

FIG. 12. Fourier transforms of the muon spin precession signal in V at $T=0.02$ K and $H<H_{c2}$.

magnetic field inhomogeneity and increases the degree of overlap of the wave functions of the core states of neighboring vortices.

The magnetic field dependence of λ in V, as determined by all three models, is plotted in Fig. 13(a). For comparison, our previously published data for V_3Si (Ref. 7) and $NbSe_2$ (Ref. 8) are shown in Fig. 13(b). In V, λ is seen to increase as a linear function of H. The value of λ determined by μSR depends on the radial decay of $B(\mathbf{r})$ outside the vortex cores. Since the spatial field profile around a vortex core can be significantly modified by the delocalization of bound core states, the measured value of λ may be strongly dependent on field. We stress that when this is the case, $\lambda(H)$ is an "effective" length scale, which in the fits absorbs changes in $B(\mathbf{r})$ due to changes in the electronic structure of the vortex lattice. This dominates over the weak field dependence of λ expected for an isolated vortex in an s-wave superconductor.[30] We note that the difference in slope of λ vs H between the models in Fig. 13 suggests that the exact details of how these changes in electronic structure are absorbed by $\lambda(H)$ is model dependent. To compare with measurements of λ by other experimental techniques, we have extrapolated the data for $\lambda(H)$ to $H\rightarrow 0$ kOe. The zero-field extrapolated value of λ in V is 376.3±22.4 Å using the iterative GL model, 375.9±17.0 Å using the analytical GL model, and 356.7±19.0 Å using the London model. Magnetization measurements[31–33] have determined that λ is in the range 374–398 Å, in excellent agreement with our results from the GL models. We therefore see that any of the three models for $B(\mathbf{r})$ can be used to extract a fairly reliable value of the zero-field magnetic penetration depth.

In V_3Si, where the bound core states are highly localized at low fields,[34] λ is weakly dependent on field below $H\approx 0.2H_{c2}$ (Ref. 7). The zero-field extrapolation shown in the inset of Fig. 13 yields λ=1080±17 Å, in good agreement with the value λ=1050 Å determined from $H_{c2}(T)$ measurements in Ref. 35. Likewise, the zero-field extrapolated value λ=1249±31 Å for $NbSe_2$ agrees well with the value of 1240 Å obtained in Ref. 36 from magnetization measurements. We note that the steep increase in λ at low fields in $NbSe_2$ is due to multiband superconductivity. Due to the smaller energy gap, at low fields there is significant delocalization of the weakly bound core states. Thus μSR can be used for accurate measurements of the absolute value of the magnetic penetration depth in type-II superconductors, provided there are sufficient data to permit an accurate extrapolation to zero field. This works even in the case of an unconventional superconductor. Recently, it was shown that zero-field extrapolated values of λ obtained from μSR measurements on the high-temperature superconductor $YBa_2Cu_3O_{6+x}$ agree well with values obtained from accurate electron spin resonance measurements in the Meissner phase.[37] We note that the linear extrapolations of the data in Fig. 13 are continuous through the Meissner phase—which occurs in V below $H_{c1}\approx 0.25H_{c2}$.

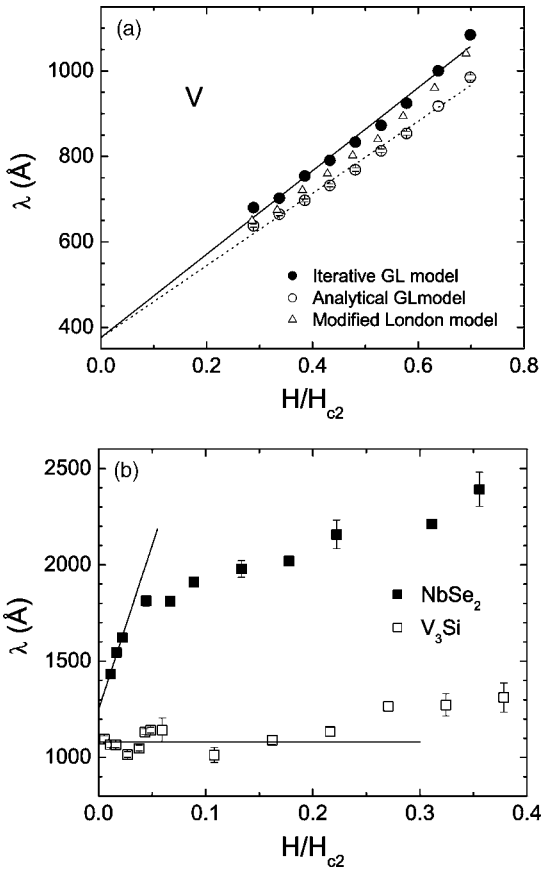

FIG. 13. μSR measurements of the magnetic field dependence of λ in (a) V, (b) V_3Si (Ref. 7) and $NbSe_2$ (Ref. 8). The straight lines are linear extrapolations of the data to zero field.

The magnetic field dependence of ξ at $T=0.02$ K is plotted in Fig. 14. Although the analytical GL model yields larger values of ξ, both GL models display a similar field dependence over the entire field range. Use of the modified London model, however, results in a stronger field depen-

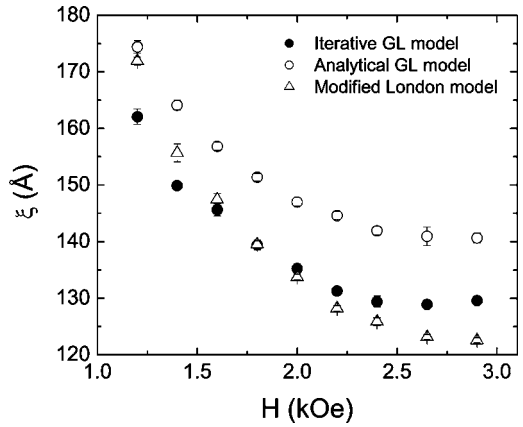

FIG. 14. Magnetic field dependence of ξ in V at $T=0.02$ K as determined from fits using the iterative and analytical GL models and the modified London model.

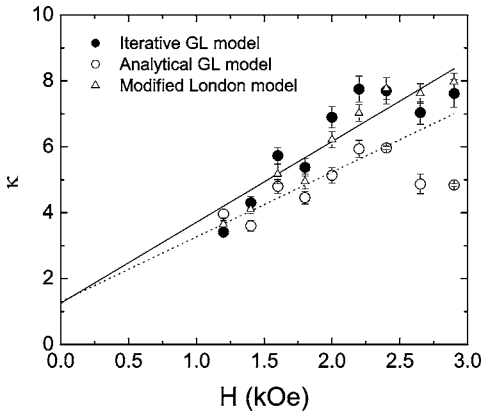

FIG. 15. Magnetic field dependence of $\kappa=\lambda/\xi$ in V at $T=0.02$ K as determined from the iterative and analytical GL models and the modified London model. The solid (dotted) line is a linear fit to the data obtained from the iterative (analytical) GL model (see main text). The fit to the data obtained from the analytical GL model excludes the points at $H=2.65$ kOe and 2.9 kOe.

dence. Regardless of the model used, it is seen that immediately above H_{c1}, the vortex core size ($\sim\xi$) shrinks with increasing field. Fits to either of the two GL models yield a saturation of $\xi(H)$ above $H\approx 2.4$ kOe, while fits to the modified London model do not. [We note that analysis of a recent Andreev reflection spectroscopy study of niobium revealed a similar trend for $\xi(H)$ over the same range of reduced fields, $0.3\leq b\leq 0.7$ (Ref. 38).] We attribute this behavior to an increase in the overlap of the core states of nearest-neighbor vortices,[39] as was found to be the case in V_3Si and $NbSe_2$.[7,8] Although Kogan and Zhelezina [40] have also successfully modeled the field dependence of the core size in V_3Si and $NbSe_2$ by weak-coupling BCS theory, their calculations assume a large GL parameter $\kappa=\lambda/\xi$ and hence are not applicable to V. In an isotropic *s*-wave superconductor, the delocalization of core states is predicted to be significant at fields above $B^*\approx B_{c2}/3$, although the value of this crossover field is reduced somewhat by anisotropy.[41] Specific heat[32] and ultrasonic attenuation[42] measurements suggest that the anisotropy of the superconducting energy gap in V is approximately 10%. According to the calculations of Ref. 41, significant delocalization of the core states and a reduction in the core size should occur above $B^*\approx 1.3$ kG. Given the uncertainty in the values of $B_{c2}(T\rightarrow 0)$ and the anisotropy, the observed shrinking of the vortex cores at fields $H\geq 1.2$ kOe seems reasonable.

Finally, we present the magnetic field dependence of the GL parameter $\kappa=\lambda/\xi$ in Fig. 15. The increase in κ with field is due to the field dependences of λ and ξ. It is evident from Fig. 15 that for all three models, κ is roughly a linear function of H. Significant deviations from this behavior occur for the values of κ at the two highest fields determined from fits to the analytical GL model. This is perhaps due to the fact that this model breaks down at high reduced fields b. It was found that both scatter and uncertainty in the values of λ and ξ were considerably reduced by fixing κ at each field to lie on a straight line fit (the fits are shown in Fig. 15 for the two GL models). The $\xi(H)$ and $\lambda(H)$ data in Figs. 13 and 14 were obtained in this way. The zero-field extrapolated values of κ determined from the straight line fits shown in Fig. 15 are 1.26 ± 1.01 for the iterative GL model and 1.30 ± 0.64 for the analytical GL model. A linear fit (not shown) to the data obtained from the modified London model yielded $\kappa(0)=0.46\pm 0.58$. We note that both of the values obtained from the GL models agree well with the value $\kappa=1.34$ calculated from our estimated values of $\lambda(H=0)$ and ξ_0. Also, within experimental uncertainty, both extrapolated values of κ are comparable with that obtained by other experimental methods for samples of similar purity.[31] On the other hand, the zero-field extrapolated value of ξ obtained from the modified London model is unreliable, leading to a poor estimate of $\kappa(0)$.

VI. SUMMARY AND CONCLUSIONS

We have analyzed μSR measurements of the internal magnetic field distribution in the vortex state of the low-κ type-II superconductor V using Brandt's iterative GL method[11] and have compared the results to those obtained from analyses using the more widely used analytical GL model of Ref. 4 and modified London model of Ref. 13. Surprisingly, the two GL models produce qualitatively similar results for both the temperature and field dependences of λ and ξ. In particular, fits to each GL model yield low-temperature, zero-field extrapolated values of λ and κ that agree with previous measurements of these quantities by other techniques. We find that the largest difference between the results using these two models occurs at high fields, where the analytical GL model is being applied outside its range of validity. The observed field dependences of λ and ξ in V are likely due to the delocalization of quasiparticle core states, as has already been established in other conventional superconductors. Overall, the results obtained with the modified London model compare less favorably to those obtained with the two GL models. For example, $1/\lambda^2(T)$ is not well described by the BCS curve and the extrapolated zero-field value of ξ does not agree as well with that obtained using other techniques.

ACKNOWLEDGMENTS

We thank E. M. Forgan and E. H. Brandt for fruitful discussions, and we are grateful to P. Dosanjh and K. Musselman for assistance with resistivity measurements. The work presented here was supported by the Natural Science and Engineering Research Council of Canada and the Canadian Institute for Advanced Research. We thank staff at TRIUMF's Centre for Molecular and Materials Science for technical assistance with the μSR experiments.

*Electronic address: jsonier@sfu.ca

[1] J. E. Sonier, J. H. Brewer, and R. F. Kiefl, Rev. Mod. Phys. **72**, 769 (2000).
[2] I. G. de Oliveira and A. M. Thompson, Phys. Rev. B **57**, 7477 (1998).
[3] J. R. Clem, J. Low Temp. Phys. **18**, 427 (1975).
[4] A. Yaouanc, P. Dalmas de Réotier, and E. H. Brandt, Phys. Rev. B **55**, 11107 (1997).
[5] Z. Hao, J. R. Clem, M. W. McElfresh, L. Civale, A. P. Malozemoff, and F. Holtzberg, Phys. Rev. B **43**, 2844 (1991).
[6] W. V. Pogosov, K. I. Kugel, A. L. Rakhmanov, and E. H. Brandt, Phys. Rev. B **64**, 064517 (2001).
[7] J. E. Sonier, F. D. Callaghan, R. I. Miller, E. Boaknin, L. Taillefer, R. F. Kiefl, J. H. Brewer, K. F. Poon, and J. D. Brewer, Phys. Rev. Lett. **93**, 017002 (2004).
[8] F. D. Callaghan, M. Laulajainen, C. V. Kaiser, and J. E. Sonier, Phys. Rev. Lett. **95**, 197001 (2005).
[9] J. E. Sonier, J. H. Brewer, R. F. Kiefl, D. A. Bonn, S. R. Dunsiger, W. N. Hardy, R. Liang, W. A. MacFarlane, R. I. Miller, T. M. Riseman, D. R. Noakes, C. E. Stronach, and M. F. White, Jr., Phys. Rev. Lett. **79**, 2875 (1997).
[10] J. E. Sonier, J. H. Brewer, R. F. Kiefl, G. D. Morris, R. I. Miller, D. A. Bonn, J. Chakhalian, R. H. Heffner, W. N. Hardy, and R. Liang, Phys. Rev. Lett. **83**, 4156 (1999).
[11] E. H. Brandt, Phys. Rev. Lett. **78**, 2208 (1997).
[12] E. H. Brandt (private communication).
[13] E. H. Brandt, J. Low Temp. Phys. **73**, 355 (1988).
[14] Goodfellow Ltd., Cambridge, UK (www.goodfellow.com).
[15] Colin M. Hurd, *The Hall Effect in Metals and Alloys* (Plenum Press, New York, 1972).
[16] Charles Kittel, *Introduction to Solid State Physics*, 8th ed. (Wiley, New York, 2005).
[17] E. M. Forgan (private communication).
[18] A. Schenck, *Muon Spin Rotation Spectroscopy: Principles and Applications in Solid State Physics* (Adam Hilger, Bristol, England, 1985).
[19] V. G. Storchak and N. V. Prokof'ev, Rev. Mod. Phys. **70**, 929 (1998).
[20] E. H. Brandt and A. Seeger, Adv. Phys. **35**, 189 (1986).
[21] E. H. Brandt, Phys. Rev. B **37**, 2349(R) (1988).
[22] B. Muhlschlegel, Z. Phys. **155**, 313 (1959).
[23] M. Tinkham, *Introduction to Superconductivity*, 2nd ed. (McGraw-Hill, New York, 1996).
[24] L. Kramer and W. Pesch, Z. Phys. **269**, 59 (1974).
[25] R. I. Miller, R. F. Kiefl, J. H. Brewer, J. Chakhalian, S. Dunsiger, G. D. Morris, J. E. Sonier, and W. A. MacFarlane, Phys. Rev. Lett. **85**, 1540 (2000).
[26] J. E. Sonier, J. Phys.: Condens. Matter **16**, S4499 (2004).
[27] N. Hayashi, Y. Kato, and M. Sigrist, J. Low Temp. Phys. **139**, 79 (2005).
[28] N. Hayashi, T. Isoshima, M. Ichioka, and K. Machida, Phys. Rev. Lett. **80**, 2921 (1998).
[29] J. E. Sonier, R. F. Kiefl, J. H. Brewer, J. Chakhalian, S. R. Dunsiger, W. A. MacFarlane, R. I. Miller, A. Wong, G. M. Luke, and J. W. Brill, Phys. Rev. Lett. **79**, 1742 (1997).
[30] J. Bardeen, Phys. Rev. **94**, 554 (1954).
[31] E. Moser, E. Seidl, and H. W. Weber, J. Low Temp. Phys. **49**, 585 (1982).
[32] R. Radebaugh and P. H. Keesom, Phys. Rev. **149**, 217 (1966).
[33] S. T. Sekula and R. H. Kernohan, Phys. Rev. B **5**, 904 (1972).
[34] E. Boaknin, M. A. Tanatar, J. Paglione, D. Hawthorn, F. Ronning, R. W. Hill, M. Sutherland, L. Taillefer, J. Sonier, S. M. Hayden, and J. W. Brill, Phys. Rev. Lett. **90**, 117003 (2003).
[35] M. Yethiraj, D. K. Christen, A. A. Gapud, D. McK. Paul, S. J. Crowe, C. D. Dewhurst, R. Cubitt, L. Porcar, and A. Gurevich, Phys. Rev. B **72**, 060504(R) (2005).
[36] J. J. Finley and B. S. Deaver, Jr., Solid State Commun. **36**, 493 (1980).
[37] T. Pereg-Barnea, P. J. Turner, R. Harris, G. K. Mullins, J. S. Bobowski, M. Raudsepp, R. Liang, D. A. Bonn, and W. N. Hardy, Phys. Rev. B **69**, 184513 (2004).
[38] L. Shan, Y. Huang, C. Ren, and H. H. Wen, Phys. Rev. B **73**, 134508 (2006).
[39] M. Ichioka, A. Hasegawa, and K. Machida, Phys. Rev. B **59**, 184 (1999).
[40] V. G. Kogan and N. V. Zhelezina, Phys. Rev. B **71**, 134505 (2005).
[41] N. Nakai, P. Miranović, M. Ichioka, and K. Machida, Phys. Rev. B **70**, 100503(R) (2004).
[42] H. V. Bohm and N. H. Horwitz, in *Proceedings of the Eighth International Conference on Low Temperature Physics*, edited by R. O. Davies (Butterworth Scientific, London, 1963), p. 191.